Journal of Solid State Chemistry 182 (2009) 2088–2095

Contents lists available at ScienceDirect

Journal of Solid State Chemistry

journal homepage: www.elsevier.com/locate/jssc

Transport and mechanical property evaluation of $(AgSbTe)_{1-x}(GeTe)_x$ ($x = 0.80, 0.82, 0.85, 0.87, 0.90$)

James R. Salvador [a,*], J. Yang [a], X. Shi [b], H. Wang [c], A.A. Wereszczak [c]

[a] Materials and Processes Laboratory, GM R&D Center, Warren, MI 48090, USA
[b] Optimal, Inc. Plymouth Township, MI 48170, USA
[c] High Temperature Materials Laboratory, Oak Ridge National Laboratory, Oak Ridge, TN 37831, USA

ARTICLE INFO

Article history:
Received 20 February 2009
Received in revised form
4 May 2009
Accepted 8 May 2009
Available online 29 May 2009

Keywords:
Thermoelectrics
Powder processing
Transport measurements
Mechanical properties
Chalcogenides

ABSTRACT

$(AgSbTe_2)_{1-x}(GeTe)_x$ (known collectively by the acronym of their constituent elements as TAGS-*x*, where *x* designates the mole fraction of GeTe) materials, despite being described over 40 years ago, have only recently been studied in greater detail from a fundamental standpoint. We have prepared a series of samples with composition $(AgSbTe_2)_{1-x}(GeTe)_x$ ($x = 0.80$, 0.82, 0.85, 0.87 and 0.90). Cast ingots of the above compositions were ground and consolidated by spark plasma sintering (SPS). Sintering conditions, specifically high applied pressures of 65 MPa and slow heating rates, were identified as important variables that lead to samples with low porosity and good mechanical strength. The resulting ingots were cut for high temperature electrical, thermal transport and mechanical property evaluation. TAGS-85 was found to have the highest *ZT* of all samples investigated ($ZT = 1.36$ at 700 K) as a result of its very low value of thermal conductivity. Hall effect measurements performed from 5 to 300 K found these materials to have complex multi-band transport characteristics.

1. Introduction

Within the last decade the field of thermoelectrics has been reinvigorated by reports of several new materials advances which have the potential for high efficiency heat to electricity interconversion for waste heat recovery and solid state heating and cooling applications. The performance of materials for either of the above mentioned applications is governed by the thermoelectric figure of merit $Z = S^2/\rho\kappa$ where S is the Seebeck coefficient, ρ is the electrical resistivity, and κ is the thermal conductivity. The dimensionless figure of merit, ZT, can be obtained by multiplying Z by the absolute temperature (T). Higher Z values lead to more efficient materials and ultimately to more highly efficient devices. As such, the objective is to maximize the Seebeck coefficient while minimizing the electrical resistivity and thermal conductivity, a challenge since all three transport parameters are inter-related.

Of particular recent interest are so-called bulk nanocomposite thermoelectric materials which can be thought of as alloys between $AgSbTe_2$ or $NaSbTe_2$ and PbTe, and $AgSbTe_2$ and SnTe [1–3]. These materials crystallize in the NaCl structure type, and their variation in lattice parameters with composition obey Vegard's law as though they were simple alloys. Closer inspection, however, reveals considerably more complex behavior [4]. It is thought that the nanostructuring, which is produced spontaneously in these materials, is responsible for drastically lowering the thermal conductivity resulting in $ZT = 1.7$ for $AgPb_mSbTe_{m+2}$ [1] at 700 K and $ZT = 1.6$ at 650 K for $NaPb_mSbTe_{m+2}$ [2]. $AgSbTe_2$ alloyed with SnTe and GeTe with excellent ZT values have also been reported [5–8].

The related compounds $(AgSbTe_2)_{1-x}(GeTe)_x$ (known collectively by the acronym of their constituent elements as TAGS-*x*, where *x* designates the mole fraction of GeTe) were first reported in the 1960s [5] and have since been successfully deployed in radioisotope thermoelectric generators for deep space and remote applications [9]. The composition $(AgSbTe_2)_{0.15}(GeTe)_{0.85}$ (TAGS-85) was found to have the best combination of thermal and electrical transport properties and mechanical stability. The key feature of TAGS-*x* for thermoelectric applications is the very low thermal conductivity for the compositions TAGS-80 and TAGS-85 [10]. Despite being first described over 40 years ago and their widespread use, only recently have reports emerged addressing the fundamental aspects of the micro- and nanostructure of TAGS-*x* materials [11,12]. High resolution transmission electron microscopy of TAGS-85 has found extensive twinning in crystals, as well as phase and anti-phase regions which result in both spatial and compositional modulation [12]. More recently some evidence of nanocrystalline inclusions in TAGS-80 and TAGS-85 with lattice spacing distinctly different from the surrounding matrix has also emerged [13]. These inclusions are reminiscent of those found in

* Corresponding author.
E-mail address: james.salvador@gm.cm (J.R. Salvador).

0022-4596/$ - see front matter © 2009 Elsevier Inc. All rights reserved.
doi:10.1016/j.jssc.2009.05.024

$AgPb_mSbTe_{m+2}$ and $NaPb_mSbTe_{m+2}$ and are likewise implicated in the lowering of thermal conductivity, though is speculative at this point.

We present here the synthesis, powder metallurgical processing and resulting transport and mechanical properties of a series of $(AgSbTe_2)_{1-x}(GeTe)_x$ ($x = 0.80$, 0.82, 0.85, 0.87 and 0.90). A ZT value of 1.36 at 700 K for TAGS-85 was measured. In addition, we present the elastic modulus, Poisson's ratio, coefficients of thermal expansion (CTE) and resulting estimated resistance to thermal shock for these materials. The thermal shock resistance is a measure of how resistant a material, subjected to a thermal gradient or transient, will be to mechanical failure.

2. Experimental

Samples of $(AgSbTe_2)_{1-x}(GeTe)_x$ ($x = 0.80$, 0.82, 0.85, 0.87 and 0.90) were prepared by melting the elements in their stoichiometric ratios at 750 °C under a reduced atmosphere in fused silica tubes. Gentle mechanical mixing of the melt was done to ensure uniform distribution of all components. After soaking at 750 °C for 4 h the samples were water quenched to room temperature in a 500 ml water bath, and then ingots were ground and cold pressed followed by annealing at 500 °C for an additional 48 h.

The resulting compacts were reground and consolidated using spark plasma sintering (SPS) by applying a pressure of 65 MPa and heating to 500 °C at a rate of 50 °C/min then held at this temperature for an additional 5 min. Consolidation was complete at 500 °C as indicated by the onset of thermal expansion, and then the samples were allowed to cool under vacuum with pressure released. All samples produced were greater than 98% of their theoretical density. Samples consolidated with 60 MPa of applied pressure and at a lower temperature of 425 °C (to avoid Sb and Te losses) with the same heating rate were found to be only 90% dense, while using heating rates significantly higher than 50 °C/min with higher applied pressures resulted in porous samples which fractured easily and were difficult to cut with a low speed diamond wheel.

X-ray diffraction was used to screen for sample purity, to assess which crystallographic polymorph was present, and to determine the lattice parameters. All samples were found to crystallize in the rhombohedral polymorph and least-squares refinement of the lattice parameters found that, with the exception TAGS-85, the unit cell angle decreased linearly (further distorted from cubic) as the mole fraction of GeTe increased. The unit cell parameters of rhombohedral GeTe were used as a starting point for cell parameter refinements. Several reflections in the TAGS-85 could not be indexed to the target phase and were identified as elemental Ge. The reflections in TAGS-80 and TAGS-82 in the vicinity of $2\theta = 55^\circ$ are those of an as yet unidentified phase and could not be indexed to any known binary or ternary phases of the constituent elements.

Electron probe microanalysis found all samples to be predominantly composed of the target phase with stoichiometries in reasonably good agreement with this targeted. All samples are systematically low in Ag as a result of a Ag_5GeTe_4 secondary phase (stoichiometry determined by EPMA) that was found in all samples prepared, and may account for the secondary phase peaks found by powder X-ray diffraction. Table 1 lists the nominal and actual EPMA determined compositions. These stoichiometries were determined by averaging 15 different individual grains and based on the fact that the standard deviations of the average of these measurements approaches the theoretical minimum for X-ray counting statistics it was determined that all samples were homogenous [14]. Further inspection of back scattered electron images of the polished sample surfaces found the grains to be in the size range of 10–30 μm.

The Seebeck coefficient and electrical resistivity from 300 to 750 K were measured using an Ulvac ZEM-2 system. The Seebeck coefficient from 2 to 350 K was measured with a Quantum Design physical property measurement system. Thermal conductivity above 300 K was determined by measuring the thermal diffusivity (D), heat capacity (C_P) and density (d). Thermal diffusivity was measured with an Anter FL5000 laser flash diffusivity instrument. Heat capacity was determined by the ratio method with a sapphire standard by differential scanning calorimetry (DSC) performed with a Netzsch DSC 404c. The density was determined by measuring the dimensions and mass of the sample. Thermal conductivity is determined according to $\kappa = D \times C_P \times d$.

Electrical resistivity and Hall effect measurements from 5 to 300 K were performed using a cryostat equipped with a 5 T magnet and Linear Research AC bridge between 5 and 300 K. Good electrical contact to the samples was made by first electroplating Ni to the surface, then soldering contacts to the plating using Wood's metal and a H_3PO_4 etch.

Disk-shaped specimens were used for the elastic property measurements (i.e., elastic modulus and Poisson's ratio). All samples were measured in air with resonant ultrasound spectroscopy (RUS). The RUS captured the frequency spectrum at temperatures between 300 and 720 K. Frequencies of resonance were identified, and by knowing each specimen's density and dimensions the modal analysis results from the computer simulation software package ANSYS were used to determine the elastic modulus and Poisson's ratio for each temperature [15].

The coefficients of thermal expansion were measured using a dual-rod dilatometer on specimens that were in the form of rectangular prismatic bars. A sapphire rod was cut to a length identical to the nominal length of the specimens (~10 mm), and served as a standard. The rods were then heated in parallel with the sapphire standard within the dilatometer's tube furnace at a rate of 2 K/min to 773 K in flowing argon. Instantaneous elongations of both the specimen and sapphire standard were measured with linear variable differential transducers. The elongation differences between the specimen and the sapphire standard were then reduced to calculate the specimen's elongation as a function of temperature. The average CTEs were then determined by dividing total elongation per original specimen length per total change of temperature.

Table 1
List of the nominal composition, thermal conductivities (κ) Seebeck coefficients (S), electrical resistivities (ρ), carrier concentration (low field 1.0 T) and Hall mobility (μ_H).

Nominal composition	Actual composition	κ (W/m K)	S (μV/K)	ρ (mΩ-cm)	$p \times 10^{21}$ (cm^{-3})	μ_H (cm^2/V s)
$(AgSbTe_2)_{0.20}(GeTe)_{0.80}$	$(Ag_{0.80}SbTe_{1.90})_{0.20}(GeTe)_{0.80}$	1.7	80	0.561	2.03	5.12
$(AgSbTe_2)_{0.17}(GeTe)_{0.83}$	$(Ag_{0.84}Sb_{0.99}Te_{2.01})_{0.17}(GeTe)_{0.83}$	1.8	73	0.630		
$(AgSbTe_2)_{0.15}(GeTe)_{0.85}$	$(Ag_{0.85}Sb_{1.01}Te_{1.95})_{0.15}(GeTe)_{0.85}$	1.6	100	0.50	1.51	5.67
$(AgSbTe_2)_{0.13}(GeTe)_{0.87}$	$(Ag_{0.75}SbTe_{2.20})_{0.13}(GeTe)_{0.88}$	2.0	62	0.439	3.41	5.07
$(AgSbTe_2)_{0.10}(GeTe)_{0.90}$	$(AgSb_{1.04}Te_{2.32})_{0.10}(GeTe)_{0.90}$	2.2	61	0.343	3.92	4.63

All transport property values with the exception of Hall mobility are at 325 K. Hall mobility was measured at 300 K.

3. Results

Powder X-ray diffraction of the sintered products revealed that all samples prepared crystallized in the rhombohedral polymorphic structure characterized by an elongation along the body diagonal of the nominally cubic unit cell. The diffraction patterns have the characteristic bifurcation of several cubic reflections as shown in Fig. 1. Pure GeTe crystallizes in this form below 430 °C [16,17] while pure $AgSbTe_2$ is cubic over the temperature range of interest. Least-squares refinement of the lattice parameters finds that, with the exception of TAGS-85, the unit cell angle decreases with increasing mole fraction of GeTe, distorting further away from cubic. Pure GeTe has a unit cell angle of 88.17°, and for the samples investigated here the unit cell angle varies from 88.90° for TAGS-90 to 89.50° for TAGS-80. The cell angle for TAGS-85 and TAGS-87 is nearly identical at 89.15°. This implies that as the mole fraction of $AgSbTe_2$ is increased the unit cell tends to more closely resemble the cubic form in keeping with Vegard's law. The inset in the upper right hand portion of Fig. 1 illustrates the variation of the unit cell angle with the mole fraction of GeTe for all samples prepared.

Thermal expansion measurements noted discontinuities in the CTE values as a function of temperature corresponding to the onset of the rhombohedral to cubic phase transitions in all samples. TAGS-80 underwent this transition at 160 °C while TAGS-82 and TAGS-85 displayed discontinuities at 200 and 230 °C, respectively. Samples with higher GeTe content (TAGS-87 and TAGS-90) displayed similar behavior at 210 °C. The rhombohedral to cubic transition in pure GeTe is a displacitive ferroelectric transition which takes place over a temperature range from 220 to 440 °C [18]. With the exception of TAGS-85 the increased mole fraction of $AgSbTe_2$ lowers the temperature of this transition indicating a destabilization of the rhombohedral form. This finding was also reflected in the DSC data which showed large temperature dependence in the C_P of each of the samples associated with the phase transition at temperatures close to those where the discontinuities were observed in the CTE. Table 2 lists the average CTEs over the entire temperature range investigated for all samples prepared. The top panel of Fig. 2 shows the C_P as a function of temperature for all samples investigated. The first large peak is associated with the rhombohedral to cubic transition, and the second peak at higher temperature observed for all samples with the exception of TAGS-80 are associated with an as yet unknown event. The lower panel of Fig. 2 is a plot of the reduced elongation ($\Delta L/L_0$, where ΔL is the total specimen elongation and L_0 is the initial length) of the TAGS-90 specimen to illustrate the slope change which accompanies the phase change.

Significant effort was expended to identify SPS conditions that yielded highly dense materials. Samples which were consolidated at 60 MPa and 425 °C, were found to be only 90% to 95% dense. These samples were mechanically weak and possessed anomalously low CTEs. Lower sintering temperatures were attempted first due to the possibility of vapor loss of Te and Sb may occur at elevated temperatures particularly since these materials were sintered under dynamic vacuum. We have determined that sintering with higher pressures and temperatures of 65 MPa and

Table 2
List of the room temperature elastic moduli, Poisson's ratios, density, and the average coefficients of thermal expansion (CTE) for TAGS-*x* samples.

Nominal composition	Elastic modulus (GPa)	Poisson's ratio	d (g/cm^3)	CTE (ppm/K)
$(AgSbTe_2)_{0.20}(GeTe)_{0.80}$	50	0.24	6.26	13.3
$(AgSbTe_2)_{0.17}(GeTe)_{0.83}$	50	0.24	6.27	17.0
$(AgSbTe_2)_{0.15}(GeTe)_{0.85}$	50	0.24	6.13	14.0
$(AgSbTe_2)_{0.13}(GeTe)_{0.87}$	50	0.24	6.34	14.9
$(AgSbTe_2)_{0.10}(GeTe)_{0.90}$	50	0.24	6.28	14.4

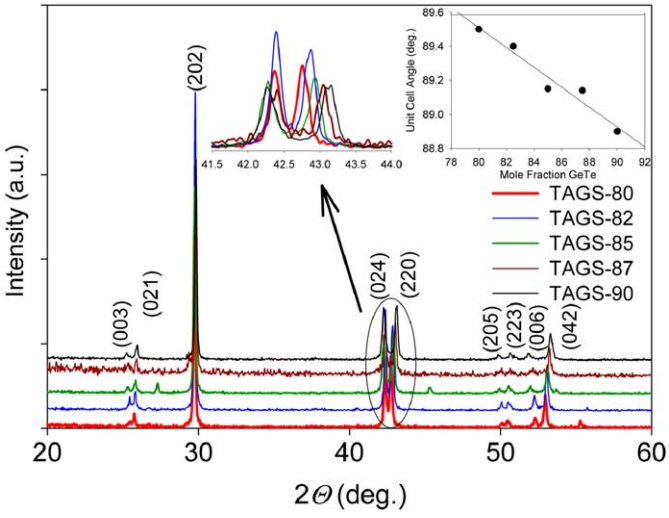

Fig. 1. Powder X-ray diffraction patterns for all samples investigated. The full patterns are indexed to the rhombohedral R 3 *m* structure. The reflection at 42° 2θ has been magnified to highlight its bifurcated nature, and the inset in the upper right-hand corner highlights the variation of the unit cell angle with GeTe content.

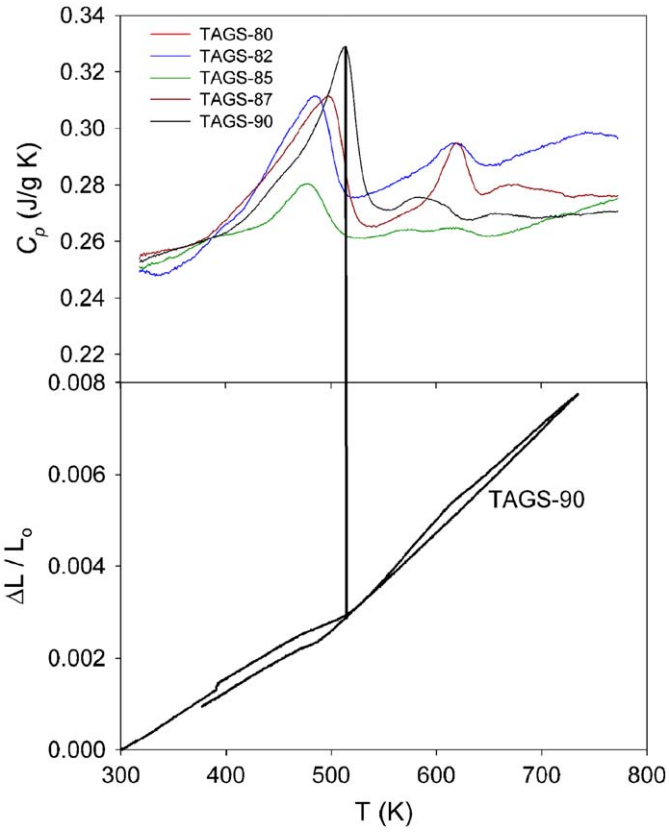

Fig. 2. The top panel shows the heat capacity (C_p) as a function of temperature for all samples investigated. The large peaks in the 400–500 K are associated with the rhombohedral to cubic phase transition. The peaks observed at higher temperature are those associated with a second transition of unknown nature. The bottom panel shows the elongation of a TAGS-90 specimen which shows a discontinuity in the slope of the $\Delta L/L_0$ with temperature (CTE). The temperature is coincident with the phase change.

500 °C lead to samples that are greater than 98% dense, are more mechanically robust, and possess CTEs comparable to those previously reported [10]. Table 2 lists the measured densities of all samples prepared with the better sintering method. Elemental analysis performed on large areas of samples (areas that would include the target and secondary phases) sinter at 500 °C find that the composition is in excellent agreement with the nominal composition indicating minimal Sb and Te loss under these conditions.

The top panel of Fig. 3 shows the electrical resistivity from 2 to 750 K. The resistivity of TAGS-80 and TAGS-87 decreases with increasing temperature in the low temperature region. Above room temperature the resistivity of all samples increases with temperature. Resistivity data below room temperature were not obtained for TAGS-82. TAGS-85 has the highest resistivity and the strongest temperature dependence, and is the only sample whose resistivity decreases at high temperature (above 700 K). The resistivity of TAGS-80 and TAGS-82 have comparable magnitude and temperature dependence above 300 K. Both display a discontinuity in ρ around 600 K, a feature that is associated with the phase transition that is evident for TAGS-82 but not observed for TAGS-80 from DSC (Fig. 2). TAGS-87 and TAGS-90 have the lowest resistivities with comparable magnitudes, and both have weak temperature dependencies. The bottom panel of Fig. 3 shows the temperature dependence of the Seebeck coefficient from 2 to 750 K which for all samples increases linearly with temperature over the entire temperature range with the exception of TAGS-85 which begins to decrease above 700 K. The linear temperature dependence of S is consistent with these materials being highly degenerate semiconductors. The values of S and ρ at 325 K are listed in Table 1. TAGS-85 has the largest Seebeck coefficient over the entire temperature range by a large margin. The Seebeck coefficients of TAGS-80 and TAGS-82 have similar magnitude and those of TAGS-87 and TAGS-90 are nearly identical, and are significantly lower than those for TAGS-80 and TAGS-82.

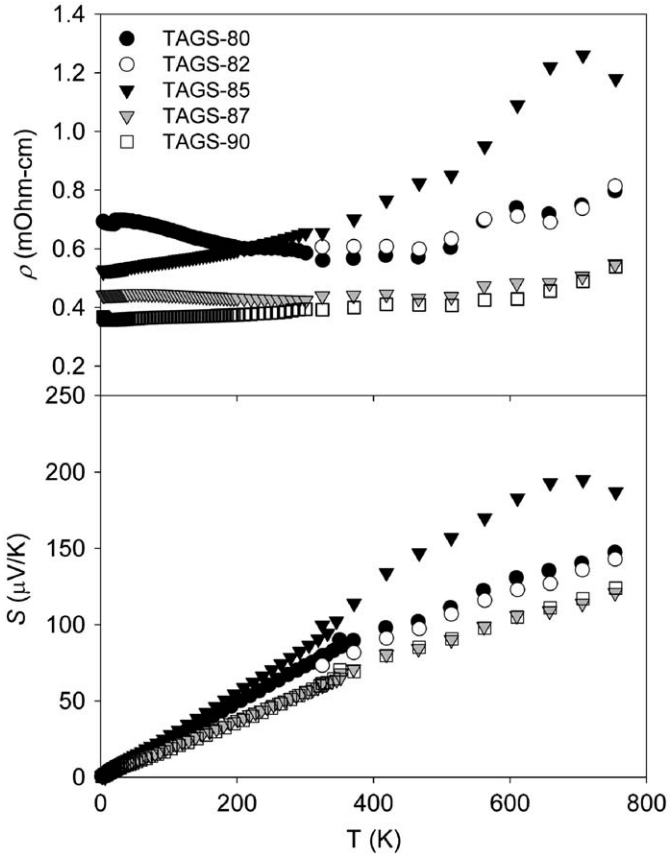

Fig. 3. Temperature dependence of electrical resistivity (top panel) and Seebeck coefficient (bottom panel) for TAGS-x between 5 and 750 K.

Fig. 4 shows the total thermal conductivity for all samples investigated. TAGS-85 possesses the lowest thermal conductivity of all samples with a room temperature value of 1.6 W/m K, a finding consistent with prior reports [10]. TAGS-85 also has weaker temperature dependence as compared to the other compositions. The κ of other samples increases with temperature as a result of the specific heat increase associated with the polymorphic phase transition. Above the transition temperatures the dependence of κ is much weaker, and aside from TAGS-85 the thermal conductivity increases with increasing mole fraction of GeTe. The very low thermal conductivities observed in TAGS-x materials are not surprising given the fact that recent reports have found the lattice thermal conductivity approaches the minimum value for $AgSbTe_2$, implying that the phonon mean free path is on the order of the phonon wavelength. The total thermal conductivity for $AgSbTe_2$ is 0.7 W/m K [19]. The κ of GeTe is significantly higher and is on the order of 4 W/m K [7]. $AgSbTe_2$ can be thought of as an end member of the pseudo-binary phase system of $AgSbTe_2$ and GeTe. The low thermal conductivity of $AgSbTe_2$ has been attributed to very large anharmonicities in the lattice vibrational spectrum leading to large phonon–phonon interactions. It is likely that similar mechanisms can be used to explain the low thermal conductivity of TAGS-x compounds. Studies have shown that the thermal conductivity of TAGS-x alloys ($x = 0.70$–0.95) increases smoothly with GeTe content with the exception of TAGS-80 and TAGS-85 which are much lower than the trend would predict [10].

Using the transport data from 325 to 750 K, ZT values can be computed for each sample. TAGS-85 is the best sample with $ZT = 1.36$ at 700 K. TAGS-80 has $ZT = 1.0$ at 750 K while TAGS-82, TAGS-87 and TAGS-90 all have comparable ZT values of ~0.8 at 750 K. Fig. 5 summarizes the temperature dependence of ZT for all samples investigated. With the exception of TAGS-85 which begins to decrease above 700 K all ZT curves increase linearly with increasing temperature up to 750 K. Literature data are also presented to show that TAGS-85 materials processed in the manner described here are comparable to those presented previously [20]. This and the fact that the thermal conductivity values measured here agree well with those reported previously

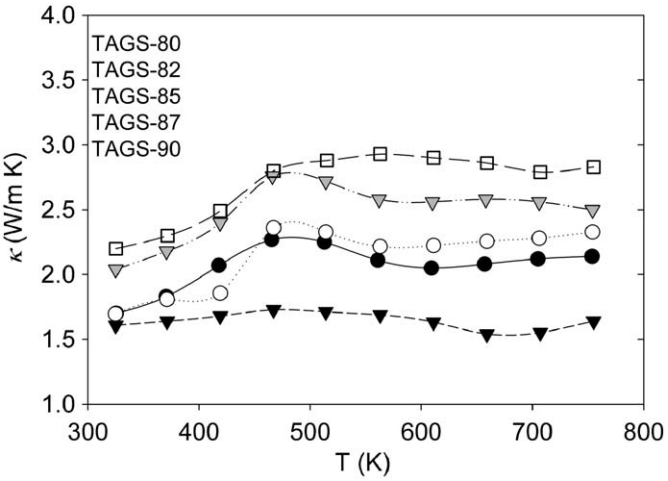

Fig. 4. Temperature dependence of the κ_{total} for all samples. Total thermal conductivity was determined by measuring the heat capacity, thermal diffusivity and density, by assuming a constant density over the range of 300–750 K.

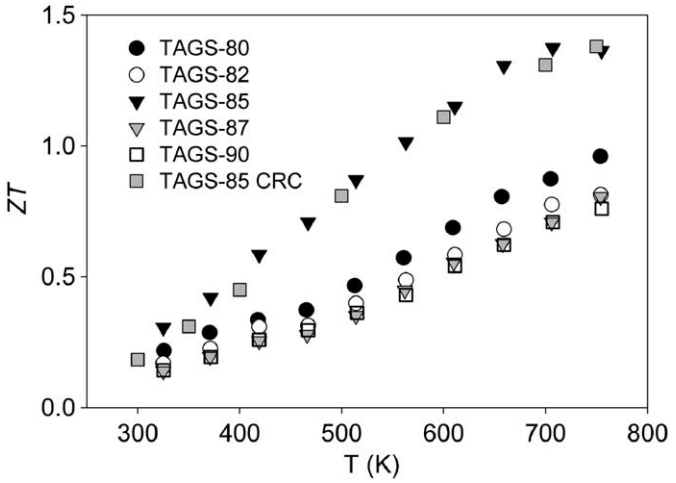

Fig. 5. Measured values of ZT for all TAGS-x samples investigated. Gray squares are literature values for TAGS-85 taken from the CRC handbook on thermoelectrics.

are important conclusions as very few actual measurements of high temperature heat capacity are performed and instead this value is either modeled through diffusivity measurements or a Dulong–Petit value (which is actually C_v) is assumed and these values are used to calculate the κ_{total}. The fact that the κ_{total} determined here from all measured values are in good agreement with these modeled values indicates the validity of their use for TAGS-x materials. Importantly the temperature dependence of κ_{total} that is associated with the phase transition is lost without the measured values of C_p. It should, however, not be assumed that this finding can be extended to other materials systems of interest. A measured value for C_P is always preferable.

Hall effect measurements found all samples to behave in a complex manner. The Hall resistance (ρ_H) was linear with magnetic field strength up to 3.0 T for TAGS-80 down to 120 K with a positive Hall coefficient (R_H). Below this temperature large departures from linear behavior were apparent, and the low field R_H's were negative indicating highly mobile electrons dominating the transport. Similar behavior (linear field dependence of ρ_H and a positive R_H) was observed for TAGS-85, though non-linear behavior did not set in until the temperature was lowered to 80 K. The non-linear behavior of the resistivity with field at 80 K is indicative of conduction taking place in multiple bands. Like TAGS-80, TAGS-85 also had a negative R_H in the low field region below 80 K. The top panel of Fig. 6 shows the Hall resistance as a function of applied field strength at several different temperatures for TAGS-85. TAGS-87 and TAGS-90 possess different behavior; near room temperature the ρ_H is non-linear with the low field slope displaying a positive R_H. As the temperature is lowered below 140 K for TAGS-87 and 200 K for TAGS-90 linearity up to fields of 3.0 T was observed for ρ_H with a positive R_H and continued down to 5 K. The bottom panel of Fig. 6 shows the behavior of the ρ_H with field for several different temperatures for TAGS-90. A recent investigation of $AgSbTe_2$ found that transport consisted of light, highly mobile electrons and heavy holes [21]. It is also known that the transport in GeTe can be understood by considering two closely spaced valence bands both of which contribute holes to conduction,[22] as a result of Ge vacancies in the lattice [23]. The room temperature carrier concentrations, assuming a single parabolic band ($p = 1/eR_H$), for the samples measured are $2.03 \times 10^{21}\,\text{cm}^{-3}$ for TAGS-80, $1.51 \times 10^{21}\,\text{cm}^{-3}$ for TAGS-85, 3.41×10^{21} and $3.92 \times 10^{21}\,\text{cm}^{-3}$ for TAGS-87 and TAGS-90, respectively. Since it is clear that conduction is taking place in multiple bands at different temperature ranges for the samples presented the value of the carrier concentration must be

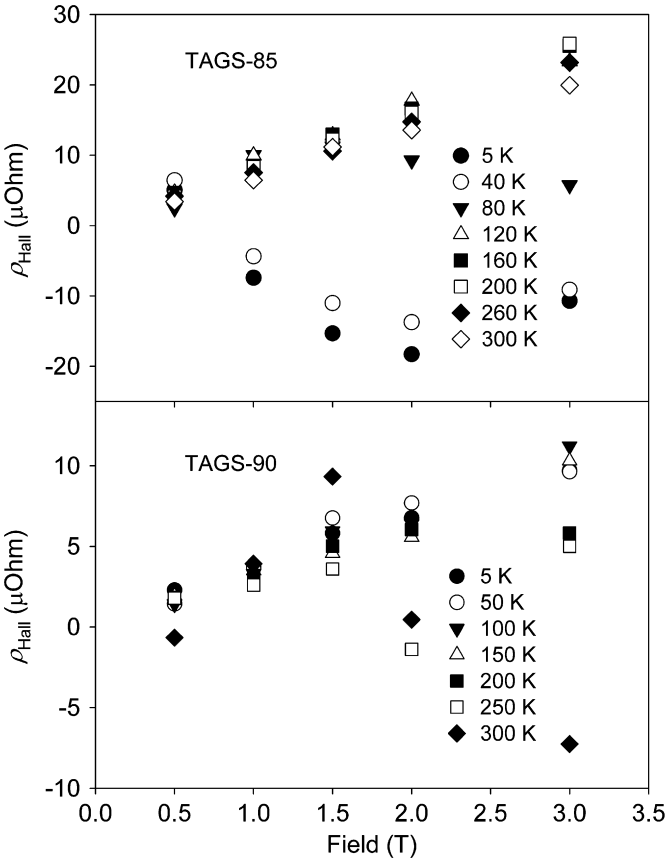

Fig. 6. Plot of ρ_H as function of magnetic field strength for TAGS-85 (top panel) and TAGS-90 bottom panel.

interpreted carefully as the primary assumption relating the Hall coefficient to the carrier concentration is that the carriers reside in a single parabolic band. The equation relating carrier concentration to R_H may have a numerator that is significantly different from unity and may be different for the different TAGS-x samples. The room temperature ρ and Hall mobilities (μ_H) are summarized in Table 1; the μ_H are all are in the range of $5.0\,\text{cm}^2/\text{V s}$, though accuracy of the mobilities is predicated on the carrier density values. Fig. 7 shows the temperature variation of μ_H for TAGS-80, TAGS-85 and TAGS-90 and the R_H for TAGS-80 and TAGS-85. The negative value for the Hall coefficient for TAGS-80 and TAGS-85 in the low temperature region indicates that electrons are the dominant charge carrier a finding at odds with the sign of the Seebeck coefficients. The mobility of carriers, shown in Fig. 7, has a T^{-1} temperature dependence which indicates a mixture of scattering mechanism. For comparison if the carriers where predominantly scattered by acoustical phonons a $T^{-3/2}$ would be expected or if ionized impurity scattering were prevalent a $T^{3/2}$ would be [24]. The T^{-1} observed for TAGS-80 and TAGS-85 may indicate a mix of these two scattering mechanism are present in these materials.

The elastic modulus, Poisson's ratio, density and coefficient of thermal expansion for all TAGS-x samples are listed in Table 2. The values for the elastic modulus and Poisson's ratio are the same for all samples (50 GPa and 0.24, respectively) and are nearly temperature independent. The coefficients of thermal expansion are consistent with those reported previously [10]. Three point bending tests performed on 5 bar shaped TAGS-85 samples found the fracture strength (ξ) to be in the range of 60 MPa. Samples used for the bend tests had a fine grain structure with porosity of 2(v/v%) based on density comparisons. The grain size distribution,

while not determined quantitatively can be estimated from SEM images to be on the order of 10's of μm, though the grain size is generally not the most important factor when considering the potential strength of a ceramic or other brittle material because larger flaws (e.g., agglomerates of grains, larger pores) are usually the strength limiters. Griffith's equation relates the strength of a material to the inverse square root of the size of its strength limiting flaw [25]. Thus the smaller the strength limiting flaw size the stronger a material can be. Fig. 8 shows the fracture surfaces and volume-type flaws that lead to specimen failure. The flaws are on the order of 500–1000 μm. If the flaws could be reduced to the size of the grains (10—30 μm) then a 5–7- fold increase in strength could be realized.

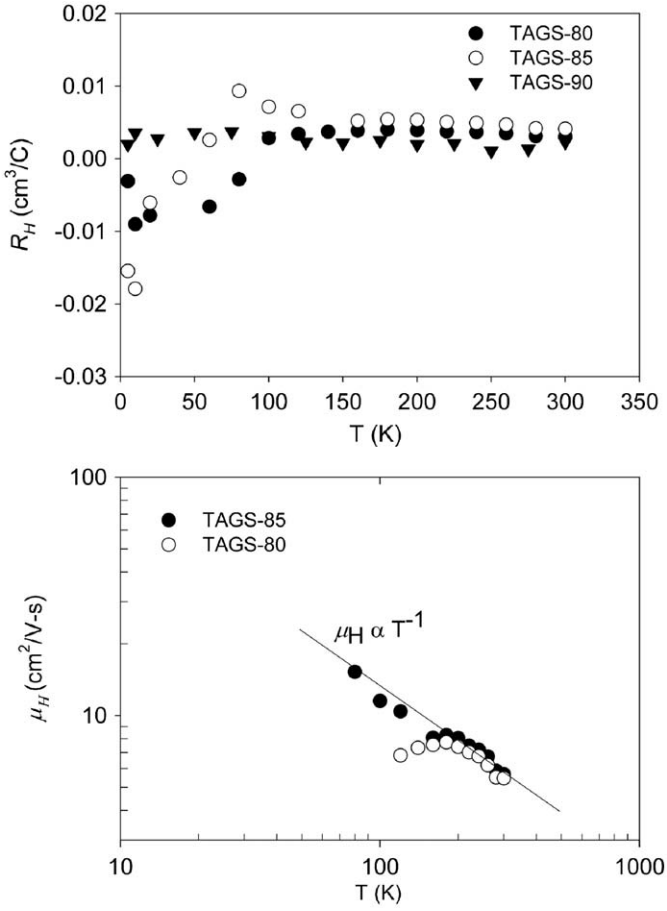

Fig. 7. The top panel shows the temperature dependence of the Hall coefficient for TAGS-80, 85 and 90. The bottom shows the Hall mobility for TAGS-80 and TAGS-85.

4. Discussion

Positive Seebeck coefficients from 2 to 750 K were found for all samples investigated. Both $AgSbTe_2$ and GeTe are known p-type semiconductors with positive Seebeck coefficients, and both are known to have electrical transport in two bands [21,22]. Hall effect measurements performed on TAGS-80 and TAGS-85 samples found that the R_H was linear with magnetic field strength in the high temperature regions and with positive ρ_H values indicating that holes are the dominate carriers, a finding that is consistent with the sign of the Seebeck coefficient. At lower temperature this linearity was no longer present, and at sufficiently low temperatures the low field R_H was negative indicating that electrons dominate charge transport despite the Seebeck coefficient being positive. Conduction in multiple bands often results in non-linear field dependence for the Hall resistance. At low temperatures a band picture similar to $AgSbTe_2$ can be envisioned for TAGS-80 and TAGS-85 such that electrical transport will be due to electrons that are in a low mass, high mobility band which will dominate the Hall coefficient. The Hall coefficient for a system with two types of carries, holes (h) and electrons (e), can be written as [26]

$$R_H = \frac{p_h\mu_h^2 - n_e\mu_e^2}{e(p_h\mu_h^2 + n_e\mu_e^2)^2}, \quad (1)$$

where p_h and n_e are the concentration of holes and electrons, respectively, μ_h and μ_e are their respective mobilities, and e is the fundamental charge. Even if there are fewer negative carriers (n_e) than positive ones (p_h), if the electron mobility is sufficiently higher than the positive carriers the R_H will be negative.

Since the Seebeck coefficient is positive at low temperatures, holes likely occupy a high effective mass band whose partial Seebeck coefficient will dominate the total thermopower. The relationship of the partial Seebeck coefficients of the different contributing bands to the total Seebeck coefficient can be expressed as $S_{\text{total}} = (S_h\sigma_h + S_e\sigma_e)/(\sigma_h+\sigma_e)$ where S_h and S_e are the hole and electron contributions to the Seebeck coefficient, respectively, and σ_h and σ_e are the respective hole and electron conductivities [27]. The partial Seebeck coefficients (S_h or S_e) can be related to their carrier concentrations (p_h and n_e) and densities of states of holes and electrons by $S_h = k_B/e(\delta_h + \ln(P_h/p_h))$ and $S_e = -k_B/e(\delta_e + \ln(N_e/n_e))$, respectively. The density of states for a parabolic band has the form P_h (or N_e) $= 2(m_{(h,e)}k_BT/2\pi\hbar^2)^{3/2}$ where $m_{(h,e)}$ is the density of states effective mass of either the hole or electron, k_B is Boltzmann's constant, and $\hbar$ is Planck's constant divided by 2π. δ_h and δ_e are terms associated with the kinetic energy of the charge carriers, and for this system can be considered equal to zero, approximating conduction in narrow bands. The relations of the partial Seebeck coefficient contributions to S_{total} (S_h and S_e) show that the magnitude of the Seebeck

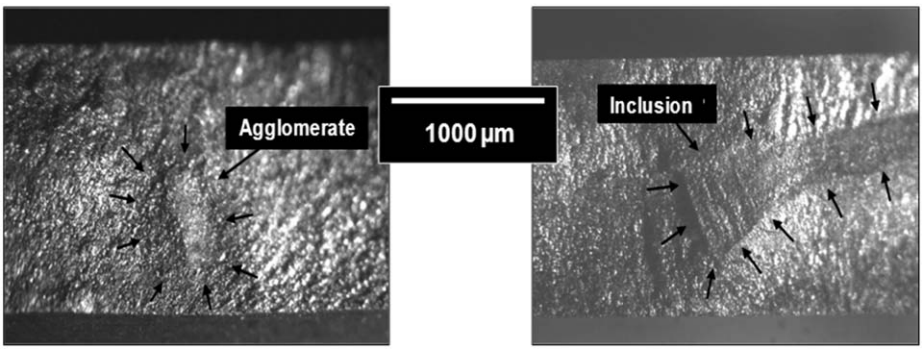

Fig. 8. Fracture surfaces of TAGS-85. In both cases agglomerations and inclusions (volume-type flaws) are responsible for the element failure.

coefficient is dependent on the number of carriers and their effective mass. A smaller number of large effective mass carriers can therefore dominate the Seebeck coefficient.

The discrepancy in the signs of low temperature R_H and S for TAGS-80 and TAGS-85 can be understood by considering a band composed of light, highly mobile electrons, and a second band composed of heavier, less mobile holes. In the high temperature limit $p_h\mu_h \gg n_e\mu_e$ in Eq. (1), and we observe R_H and S to be positive. As the temperature is lowered the terms $p_h\mu_h$ and $n_e\mu_e$ become comparable in magnitude either due to the decrease in hole carrier density or their mobility; the electron contribution becomes more pronounced, and finally becomes the dominant Hall component, and at sufficiently low temperatures $n_e\mu_e \gg p_h\mu_h$, and $R_H<0$. The Seebeck coefficients for TAGS-80 and TAGS-85 remain positive over the entire temperature range likely due to the comparatively large effective mass of the hole band. The pronounced shift from hole dominated conduction to mixed conduction takes place at 120 K for TAGS-80 and at 80 K for TAGS-85 this is illustrated by the non-linear relation of the Hall resistance to magnetic field as shown for TAGS-85 in Fig. 6. As the mole fraction of GeTe is increased further (TAGS-87 and TAGS-90), temperature dependent behavior of R_H changes, and in the high temperature region R_H is no longer linear with field, though in the low field region the slope is still positive. It is likely that as the mole fraction of GeTe is increased the two valence bands of GeTe begin to dominate the behavior of the system especially at low temperatures [22]. It has been shown before that the second valence band in pure GeTe makes a significant contribution when the carrier concentration is greater than $1.5\times10^{20}(\mathrm{cm}^{-3})$ [22]. For the samples with higher GeTe content the electronic contribution to R_H and S is much less pronounced than is the TAGS-85 and TAGS-80 examples as the sign of the these coefficients are the same.

No good structural model exists for TAGS-x compounds. It is known that these alloys adopt the rhombohedral structure at low temperatures (X-ray diffraction), but details of atomic arrangements and any long range order of the constituent atoms is lacking. As a result a reliable band structure model is also lacking. Band structures of the pseudobinary phase end members of the TAGS-x series (i.e., $AgSbTe_2$ and GeTe) find $AgSbTe_2$ has a band picture similar to that proposed for TAGS-80 and TAGS-85 [28], while the higher mole fraction samples of TAGS-87 and TAGS-90 behave more like GeTe [22].

In addition to good thermoelectric properties, good mechanical stability must also be sought for candidate materials in module design. For this, the thermal shock resistance parameter is a good measure of a material's thermomechanical potential and is expressed as

$$R_T = \frac{\xi(1-\upsilon)\kappa}{\alpha\cdot E}, \tag{2}$$

where ξ is the fracture or tensile stress, ν is Possion's ratio, κ the thermal conductivity, α the CTE, and E the elastic modulus [29]. Materials which are subject to a thermal gradient will have areas where thermal expansion is significantly greater than other areas, and this can lead to a net shape change in the component. Thermal gradients thus result in stresses within the member due to the shape change. If the element is composed of multiple grains or phases it can lead to inter-grain and inter-phase strains. These strains, if they become sufficiently large, can lead to cracks and, ultimately, failure of the element. Good thermoelectric materials, by their nature, have low κ, are generally quite brittle and have moderate to large CTE which results in unfavorable contributions to the thermal shock resistance parameter. The fracture strength ξ the only parameter that is tangibly modifiable, and it is sensitive to the microstructure and more specifically, the flaw population. This is why effort was expended to improve sintering conditions here which will, potentially, lead to mechanically stronger materials with resulting higher resistance to thermal stress. If a strength of 60 MPa is assumed for all materials, and the experimentally determined values of E, υ, α and κ are substituted in Eq. (2) the thermal shock resistances are 137, 104, 154 and 140 for TAGS-80, TAGS-85, TAGS-87 and TAGS-90, respectively. The R_T value for TAGS-85 is comparable to p-type PbTe [30]. Therefore TAGS-85 has a comparable resistance to thermal shock as p-type PbTe (with a comparable fracture strength, ξ), but with a higher ZT value in the temperature range of interest. The thermal shock resistance parameters presented here should not be considered optimal. Inspection of the fracture surfaces of TAGS-x samples found large inclusions and cracks which led to the element's failure, through better control of powder processing it could be possible to limit the flaw sizes to the range of the grain size leading to significant improvement in strength and thermal shock resistance.

5. Summary and conclusions

A series of TAGS-x samples has been synthesized and consolidated by SPS. The electrical transport properties of TAGS-80 and TAGS-85 can be understood by a 2 band model of light, highly mobile electrons and heavy holes. The hole band in these samples becomes dominant at high temperatures. TAGS-87 and 90 by contrast have 2 valence bands which are competing at high temperatures with a much smaller contribution from the conduction bands, and as the samples are cooled one band becomes dominant and the Hall coefficient behaves as though there is a single band. TAGS-85 is the best sample with $ZT = 1.36$ at 700 K. All samples have an elastic modulus of 50 GPa and an a Poisson's ratio of 0.24. The resulting R_T values for the TAGS-x samples are comparable to p-type PbTe meaning these TAGS-x materials will behave comparably to PbTe in a temperature gradient.

Acknowledgments

J.R.S., X.S. and J.Y. would like to thank Drs. J.F. Herbst and M.W. Verbrugge for their continued support and encouragement. The work is supported by GM and by DOE under corporate agreement DE-FC26-04NT42278, by the Assistant Secretary for Energy Efficiency and Renewable Energy, Office of Transportation Technologies as part of the High Temperature Materials Laboratory User Program at Oak Ridge National Laboratory managed by the UT-Battelle LLC, for the Department of Energy under contract DEAC05000OR22725.

References

[1] K.F. Hsu, S. Loo, F. Guo, W. Chen, J.S. Dyck, C. Uher, T. Hogan, E.K. Polychroniadis, M.G. Kanatzidis, Science 303 (2004) 818–821.
[2] P.F.P. Poudeu, J. D' Angelo, A.D. Downey, J.L. Short, T.P. Hogan, M.G. Kanatzidis, Angew. Chem. Int. Ed. 45 (2006) 3835–3839.
[3] J. Androulakis, R. Pcionek, E. Quarez, J.H. Do, J.H. Kong, O. Palchik, C. Uher, J.J. D'Angelo, J. Short, T. Hogan, M.G. Kanatazidis, Chem. Mater. 18 (2006) 4719–4721.
[4] E. Quarez, K.F. Hsu, R. Pcionek, N. Frangis, E.K. Polychroniadis, M.G. Kanatzidis, J. Am. Chem. Soc. 127 (2005) 9177–9190.
[5] D. Rosi, J.P. Dismuke, E.F. Hockings, Electr. Eng. 79 (1960) 450–459.
[6] J.H. Wernick, H.C. Gatos (Eds.), Properties of Elemental and Compound Semiconductors, Interscience, New York, 1960 p. 69.
[7] C. Wood, Rep. Prog. Phys. 51 (1988) 459–539.
[8] S.K. Placheova, Phys. Stat. Sol. A 83 (1984) 349–355.
[9] G.L. Bennett, in: D.M. Rowe (Ed.), CRC Handbook of Thermoelectrics, CRC Press, Boca Raton, 1995, p. 515.
[10] E. Skrabek, D. Trimmer, US Patent No. 3,945,855, March 23, 1976.

[11] B.A. Cook, M.J. Kramer, X. Wei, J.L. Harringa, E.M. Levin, J. Appl. Phys. 101 (2007) 053715.
[12] B.A. Cook, X. Wei, J.L. Harringa, M.J. Kramer, J. Mater. Sci. 42 (2007) 7643–7646.
[13] S.H. Yang, T.J. Zhu, T. Sun, J. He, S.N. Zhang, X.B. Zhao, Nanotechnology 19 (2008) 245707.
[14] M. Anecy, F. Bastenaire, R. Trixier, Applications of statistical methods in microanalysis, in: F. Maurice, L. Meny, R. Tixier (Eds.), Microanalysis and Scanning Electron Microscopy, Les Éditions de Physique Les Ulis, Orsay, 1978, p. 319.
[15] A.A. Wereszczak, Ceram. Eng. Sci. Proc. 7 (2006) 211–220.
[16] J.Y. Raty, J.-P. Gaspard, C. Bichara, C. Bergman, R. Bellissent, R. Ceolin, Physica B 276 (2000) 473–474.
[17] J. Goldak, C.S. Barrett, D. Innes, W. Youdles, J. Chem. Phys. 44 (1966) 3323–3325.
[18] T. Chattopadhyay, J.X. Boucherle, G.G. von Schnering, J. Phys. C. Solid State Phys. 20 (1987) 1431–1440.
[19] D.T. Morelli, V. Jovovic, J.P. Heremans, Phys. Rev. Lett. 101 (2008) 035901.
[20] E.A. Skrabeck, D.S. Trimmer, in: D.M. Rowe (Ed.), CRC Handbook of Thermoelectrics, CRC Press, Boca Raton, 1995, p. 272.
[21] V. Jovovic, J.P. Heremans, Phys. Rev. B 77 (2008) 245204.
[22] N.V. Kolomiets, E.Ya. Lev, L.M. Sysoeva, Sov. Phys. Solid State 6 (1965) 551–560.
[23] A.H. Edwards, A.C. Pineda, P.A. Schultz, M.G. Martin, A.P. Thompson, H.P. Halmarson, C.J. Umrigar, Phys. Rev. B 73 (2006) 045210.
[24] G.A. Slack, M.A. Hussain, J. Appl. Phys. 70 (1991) 2694.
[25] A.A. Griffith, Phil. Trans. Roy. Soc. London 221A (1920) 163–198.
[26] O.V. Emel'yanenko, T.S. Lagunova, D.N. Nasledov, G.N. Talalakin, Sov. Phys. Solid State 7 (1965) 1063–1069.
[27] A.F. Ioffe, Physics of Semiconductors, Infosearch Limited, London, 1960.
[28] K. Hoang, S.D. Mahanti, J.R. Salvador, M.G. Kanatzidis, Phys. Rev. Lett. 99 (2007) 156403.
[29] W.D. Kingery, J. Am. Ceram. Soc. 38 (1959) 3–15.
[30] A.A. Wereszczak, J.R. Salvador X. Shi, J. Yang, unpublished.